Out-of-plane optical conductivity measured in bilayer graphene

Yu He,[1,2] Davide Ferraro,[1] Zhemi Xu,[1,3] Leonardo Cobelli,[1] Luca Dell'Anna,[1] Alessandro Martucci,[4] Paolo Umari,[1,5] and Michele Merano[1,*]

[1]*Dipartimento di Fisica e Astronomia "Galileo Galilei", Università degli Studi di Padova, IT-35131 Padova, Italy*
[2]*College of Optoelectronic Engineering, Chengdu University of Information Technology, Chengdu 610225, China*
[3]*College of Chemistry and Materials Engineering, Beijing Technology and Business University, Beijing 100048, China*
[4]*Dipartimento di Ingegneria Industriale and INSTM, Università degli Studi di Padova, IT-35131 Padova, Italy*
[5]*CNR-IOM–Istituto Officina dei Materiali, National Research Council of Italy, c/o SISSA Via Bonomea 265, IT-34136 Trieste, Italy*

(Received 3 October 2023; revised 16 April 2024; accepted 6 May 2024; published 30 May 2024)

We report the experimental observation of the out-of-plane optical conductivity in bilayer graphene at a wavelength of 633 nm. While the in-plane optical constants vary by a few percent from the single-layer crystal up to the bulk, this physical quantity depends strongly on interlayer interactions, being at least three times larger in bilayer than in monolayer graphene.

DOI: 10.1103/PhysRevA.109.053530

I. INTRODUCTION

Two-dimensional (2D) materials, with atomic thickness and macroscopic lateral dimensions, are often modeled as optically isotropic slabs [1–3]. This appears to be in conflict with their atomic structure and with the optical anisotropy of their three-dimensional precursors [3–7]. For instance, bulk hexagonal boron nitride is a transparent negative uniaxial crystal [8]. Both ordinary and extraordinary complex dielectric functions of graphite show nonzero absorption in the visible spectrum [5]. Large optical anisotropy was recently observed in bulk transition-metal dichalcogenides (TMDCs) with important applications for on-chip next-generation photonics [7].

The reason why the isotropic slab model is so successful in describing 2D crystals is because the out-of-plane optical constants of these materials are experimentally elusive quantities. This was soon recognized by scientists performing ellipsometric experiments on graphene [9]. The substrate on which 2D materials are deposited hides the contribution due to the out-of-plane optical constants. Indeed, the sensitivity of optical measurements to anisotropy depends on the path length of the light through the material, which is extremely limited for monolayers or few-layer crystals [9]. There is much experimental evidence for this. Since the discovery of 2D crystals, the number of optical experiments (not only ellipsometry) performed on them is enormous. Still, we lack information on their birefringence.

The quest for the magnitude of the out-of-plane optical constants of 2D crystals has been recently addressed. Both analytical and *ab initio* theoretical approaches suggest that these physical quantities should be different from their in-plane counterparts [10–15]. From an experimental point of view, the observation of the out-of-plane surface susceptibility of monolayer graphene was reported [16,17]. The light reflected from the substrate (that hides the contribution from the out-of-plane optical constants) was removed by immersion of a monolayer in the middle of a bulk transparent polymer prism. Experimental data confirm that graphene is an anisotropic material.

By contrast with the out-of-plane properties, the in-plane optical constants of 2D crystals are experimentally accessible. They can be measured via ellipsometry [18–20], via reflectivity and transmissivity measurements [21], or optical contrast [22]. The number of experiments concerning the in-plane optical constants of graphene is impressive. Nair *et al.* observed that, for visible photon energies, multilayer graphene can be considered as a stack of independent atomic planes [23]. As a result, the obtained in-plane optical constants of graphene could also be used (with errors of a few percent) for bilayer, trilayer, and multilayers up to graphite [5,23–26]. In technical language, the in-plane sheet susceptibility ($\chi_\parallel$) and conductivity ($\sigma_\parallel$) of graphite are very close to the in-plane surface susceptibility and conductivity of graphene. Bora and Borini ascribed this behavior to the relatively low value of the interlayer hopping term in multilayered graphene, which is negligible when transition energies in the visible range are being probed [26].

While the in-plane optical constants of graphene resemble graphite's ones, the out-of-plane constants of the monolayer seem considerably smaller than those of the bulk precursor [16,17]. Experimental data for graphite [5] suggest that the out-of-plane sheet susceptibility ($\chi_\perp$) and conductivity ($\sigma_\perp$) of this material are very different than the out-plane surface susceptibility and conductivity of graphene. In particular this last optical constant is too small to be observed with the present experimental sensitivity [16,17]. Were it similar to its bulk precursor, it would have been largely observable. In view of these considerations, it is of the utmost importance to study how the out-of-plane optical constants vary with the number of layers. To this end, we report an experimental measurement

*michele.merano@unipd.it

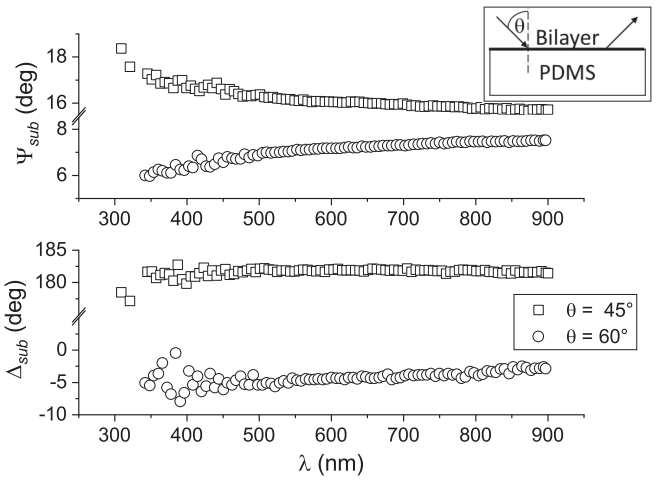

FIG. 1. Spectroscopic ellipsometric parameters of bilayer graphene deposited on PDMS. The experimental data refer to two different angles of incidence $\theta = 45^\circ$ and $\theta = 60^\circ$.

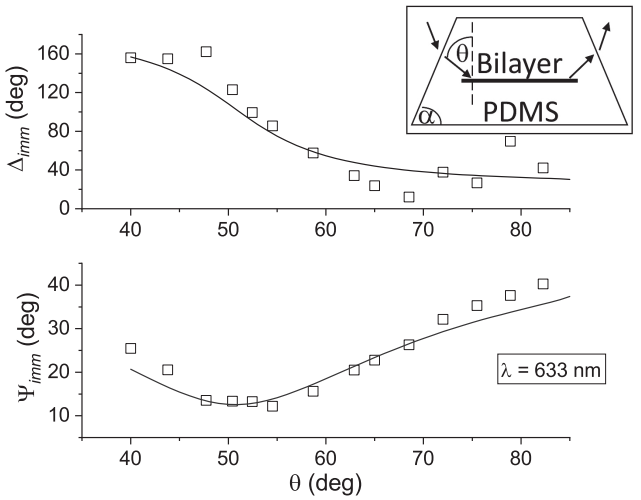

FIG. 2. Ellipsometric parameters of bilayer graphene immersed in PDMS at $\lambda = 633$ nm. Dots: Experimental data. Lines: Theoretical predictions assuming for the optical constants the values reported in Table I.

of the optical constants of bilayer graphene for comparing to the monolayer [16,17].

II. EXPERIMENTAL PROCEDURE

Standard ellipsometry cannot separate the in-plane, the out-of-plane, and the substrate contributions to the reflection of a 2D crystal even if we allow the angle of incidence to vary. For this reason, we adopt a two-step approach that was already successful for monolayer graphene [16,17].

The first step consists in a standard ellipsometric experiment. A bilayer graphene sample, with lateral dimensions of the order of 1 cm, grown by chemical vapor deposition, is deposited on a transparent polydimethylsiloxane (PDMS) substrate (graphene films on PDMS were purchased from the Beijing Graphene Institute). The inset in Fig. 1 shows schematically the sample studied. The arrows indicate the incident and the reflected light direction. We use a commercial spectroscopic ellipsometer (VASE®, J. A. Woollam) to measure the complex ratio,

$$\frac{r_{\mathrm{p\_sub}}}{r_{\mathrm{s\_sub}}} = \tan(\Psi_{\mathrm{sub}})e^{i\Delta_{\mathrm{sub}}}, \tag{1}$$

of the reflection coefficients $r_{\mathrm{p\_sub}}$ for p and $r_{\mathrm{s\_sub}}$ for s-polarized incident light.

In a second step, we remove the substrate contribution. We place the same sample used in the first step of the experiment in a prism-shaped mold (base 6×5 cm, height 3.5 cm), pour nonpolymerized PDMS on it, and wait for complete polymerization. Owing to the replicant properties of PDMS we obtain a bilayer graphene totally immersed in the PDMS prism without spurious interfaces. This was carefully verified experimentally by preparing PDMS prisms without the bilayer graphene. There is no interface in between the previous and the newly added material in this case. The angle α at the base of the prism (see the inset in Fig. 2) has a value of 65°. The geometry of the prism has been chosen to measure at angles of incidence greater than 45° where the out-of-plane optical constants play a more relevant role. In this second step, the light reflected from the sample is much less than in the previous experiment. This forced us to develop a homemade ellipsometric setup (for a complete description, refer to Ref. [16]) to measure the complex ratio,

$$\frac{r_{\mathrm{p\_imm}}}{r_{\mathrm{s\_imm}}} = \tan(\Psi_{\mathrm{imm}})e^{i\Delta_{\mathrm{imm}}}, \tag{2}$$

of the reflection coefficients at a vacuum wavelength (λ) of 633 nm.

Figure 1 reports the ellipsometric parameters Δ_{sub} and Ψ_{sub}, for bilayer graphene deposited on a transparent PDMS substrate as a function of λ. Measurements are taken in all the visible spectra at two different angles of incidence θ: 45° and 60°. These two angles have been chosen below and above the Brewster angle for PDMS (54.07° at 633 nm). For this reason Δ_{sub} assumes values close to 180° at $\theta = 45^\circ$ and values close to 0° at $\theta = 60^\circ$. We observe that Ψ_{sub} is a monotonically decreasing function for $\theta = 45^\circ$ and it is a monotonically increasing function for $\theta = 60^\circ$.

Figure 2 reports the ellipsometric parameters Δ_{imm} and Ψ_{imm}, for bilayer graphene immersed in a PDMS prism as a function of the incident angle (θ) on the bilayer (the inset in Fig. 2 schematically shows the direction of the incident and the reflected light by the sample). Measurements at different θ verify that the optical constants do not depend on θ and on a specific position on the sample.

Figure 3 reports the intensity reflectivities $R_{\mathrm{s\_imm}} = |r_{\mathrm{s\_imm}}|^2$ and $R_{\mathrm{p\_imm}} = |r_{\mathrm{p\_imm}}|^2$ for s- and p-polarized light incident at θ on the bilayer immersed in PDMS. While $R_{\mathrm{s\_imm}}(\theta)$ is a monotonically increasing function, $R_{\mathrm{p\_imm}}(\theta)$ shows a minimum at the pseudo-Brewster angle θ_{pB}. If we compare these data with the experimental data for monolayer graphene [16] we note two items. The first is that $R_{\mathrm{s\_imm}}$ is approximately four times larger in bilayer than in monolayer graphene. This is expected because $R_{\mathrm{s\_imm}}$ depends only on the in-plane optical constants and in this case, as observed by Nair *et al.* [23], bilayer graphene can be considered as a stack

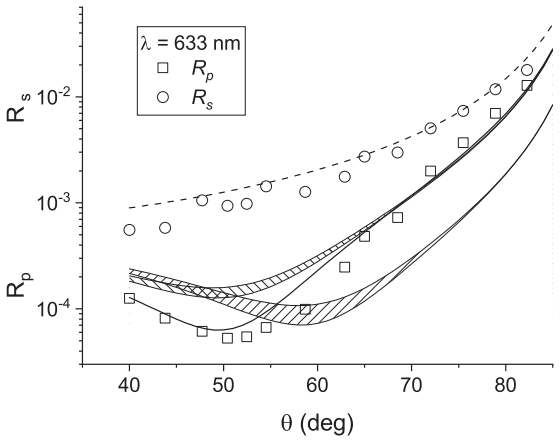

FIG. 3. Intensity reflectivity for *s*- and *p*-polarized light of bilayer graphene immersed in PDMS at $\lambda = 633$ nm. Circle (square) dots: Experimental data for *s* (*p*) polarization. Solid and dashed lines: Theoretical predictions assuming for the optical constants the values reported in Table I. Patterned area at -45°: The theoretical predictions for $R_{\mathrm{p\_imm}}(\theta)$ if we set $\sigma_\perp$ compatible with our observations for the monolayer. Patterned area at 45°: The theoretical predictions for $R_{\mathrm{p\_imm}}(\theta)$ if we set bot $\sigma_\perp$ and $\chi_\perp$ compatible with our observations for the monolayer.

of two independent monolayer graphene planes. Two layers of graphene reflect twice a single layer and the reflectivity is proportional to the square of the reflected amplitude. Second, we observe that for monolayer graphene immersed in a dielectric medium $\theta_{\mathrm{pB}} = 56.5^\circ$ [16], while here we observe $\theta_{\mathrm{pB}} = 50^\circ$. The behavior of *p*-polarized light is strikingly different from *s*-polarized light and it deserves an explanation.

III. THEORETICAL MODEL

To extract the optical constants of bilayer graphene from the experimental data we need a theoretical model that provides the correct reflection coefficients for it. Usually, in the literature, 2D crystals are modeled as isotropic or anisotropic slabs [1,27], but this oversimplified approach does not work for 2D crystals immersed in a dielectric medium. We tried this model [28] for bilayer graphene but, as for the monolayer [16], we obtain a negative out-of-plane susceptibility that looks unphysical and in contrast with *ab initio* calculations [11,12] (see below).

A convenient model was developed in Refs. [29,30]. In brief, if we consider two graphene monolayers separated by a distance much greater (five times greater is largely enough) than the linear dimensions of the unit cell of graphite, the interaction in between the two atomic planes is completely negligible and they can be considered as completely independent monolayers. Given an incident electromagnetic field, it is possible to define a reflected and a transmitted field and two electromagnetic fields in between the two monolayers (Fig. 4). The optical constants of these two atomic planes are equal to those of an isolated monolayer.

If we let the distance of the two monolayers become smaller and smaller (Fig. 4), down to the interlayer distance of the bilayer graphene ($d = 0.33$ nm), the interaction of the two atomic planes is no longer negligible. The approach

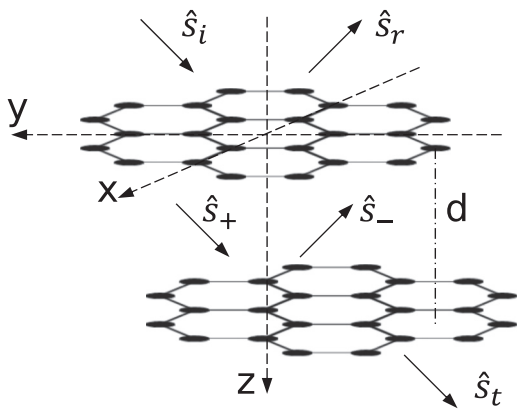

FIG. 4. Oblique incidence of a plane wave on bilayer graphene. The unit vectors $\hat{s}_{i(r,t,+,-)}$ give the propagation direction of the electromagnetic fields. The subscript i (r, t) stands for the incident (reflected, transmitted) field. The subscripts $+$ and $-$ refer to the electromagnetic fields in between the two atomic layers.

just described remains valid, and it is still possible to define common $\chi_\parallel$, $\chi_\perp$, $\sigma_\parallel$, $\sigma_\perp$ for the two atomic planes, but their values differ from those of an isolated monolayer.

We consider an incident plane wave (Fig. 4), with propagation direction $\hat{s}_i = (0, -\sin\theta, \cos\theta)$ and time dependence $e^{i\omega t}$ (ω is the angular frequency of the light). For a bilayer graphene immersed in PDMS we have $\hat{s}_i = \hat{s}_+ = \hat{s}_t$, $\hat{s}_r = \hat{s}_- = (0, -\sin\theta, -\cos\theta)$, and the magnetic fields are related to the electric ones via $\frac{\eta}{n}\vec{H}_a = \hat{s}_a \times \vec{E}_a$ where a can be either $(i, r, t, +, -)$.

This wave generates surface polarizations $\vec{P}_{1(2)}$ on the two graphene planes (denoted by the subscripts 1 and 2) that form the bilayer. We have

$$\begin{pmatrix} P_{1(2)x} \\ P_{1(2)y} \\ P_{1(2)z} \end{pmatrix} = \epsilon_0 \begin{pmatrix} \chi_\parallel & 0 & 0 \\ 0 & \chi_\parallel & 0 \\ 0 & 0 & \chi_\perp \end{pmatrix} \begin{pmatrix} E_{1(2)x} \\ E_{1(2)y} \\ E_{1(2)z} \end{pmatrix}, \tag{3}$$

where $\vec{E}_{1(2)}$ are the macroscopic electric fields at the two atomic planes and ϵ_0 is the vacuum permittivity. The same wave generates also the surface ohmic currents $\vec{J}_{1(2)}$,

$$\begin{pmatrix} J_{1(2)x} \\ J_{1(2)y} \\ J_{1(2)z} \end{pmatrix} = \begin{pmatrix} \sigma_\parallel & 0 & 0 \\ 0 & \sigma_\parallel & 0 \\ 0 & 0 & \sigma_\perp \end{pmatrix} \begin{pmatrix} E_{1(2)x} \\ E_{1(2)y} \\ E_{1(2)z} \end{pmatrix}. \tag{4}$$

For a *p*-polarized wave we have $E_{1(2)x} = 0$, $P_{1(2)x} = 0$, $J_{1(2)x} = 0$. This wave generates on each atomic plane total in-plane surface currents given by $i\omega P_{1(2)y} + J_{1(2)y}$ and total out-of-plane surface currents given by $i\omega P_{1(2)z} + J_{1(2)z}$. The total reflected field is a linear superposition of the reflected fields generated by these in-plane and out-of-plane surface currents [10,16], so the reflection coefficient for *p*-polarized light can be expressed as a sum $r_{\mathrm{p\_imm}} = r_{p\parallel} + r_{p\perp}$.

For an *s*-polarized incident wave, only $E_{1(2)x}$ is different from zero [Eqs. (3) and (4)]. This wave excites only in-plane surface polarizations $P_{1(2)x}\hat{i}$ and in-plane ohmic surface currents $J_{1(2)x}\hat{i}$. We show how to derive the reflection coefficients in the Appendix.

TABLE I. Optical constant of bilayer graphene at $\lambda = 633$ nm. Data are compared with their analogs for monolayer graphene [16] and graphite [31].

	$\chi_\parallel$ (nm)	$\sigma_\parallel$ (10^{-5} Ω^{-1})	$\chi_\perp$ (nm)	$\sigma_\perp$ (10^{-5} Ω^{-1})
Monolayer	1.7 ± 0.2	6.8 ± 0.3	0.6 ± 0.2	0.3±0.3
Bilayer	2.0 ± 0.3	6.8 ± 0.5	1.1 ± 0.2	1.1±0.4
Graphite	1.7	6.9	0.9	2.2

IV. DATA ANALYSIS

With MATHEMATICA it is easy to solve the linear equation systems giving the Fresnel reflection coefficients for the bilayer graphene immersed in PDMS or deposited on a PDMS substrate (see the Appendix). Then, using the data of Figs. 1 and 2, we numerically invert the fundamental equations of ellipsometry Eqs. (1) and (2) and we recover the optical constants of this material at $\lambda = 633$ nm.

The experimental data in Figs. 2 and 3 are the raw data. They include the initial transmission from air to PDMS, the reflection on the bilayer, and the subsequent transmission from PDMS to air. PDMS is a transparent dielectric, so we measured for it a real refractive index $n = 1.38$ at $\lambda = 633$ nm. Transmission through a transparent material does not affect $\Delta_{\rm imm}$. In the data analysis we include the small contribution to $\Psi_{\rm imm}$, $R_{\rm s\_imm}$, and $R_{\rm p\_imm}$ of the transmissions through the two prism sides.

Table I compares the experimental data for monolayer [16] and bilayer graphene with those for bulk graphite [31]. As for Ref. [16], data in Ref. [31] are also confirmed by *ab initio* calculations [11,32]. We note that $\chi_\parallel$ and $\sigma_\parallel$ for the bilayer are practically equal to the values measured for monolayer graphene, while $\chi_\perp$ and $\sigma_\perp$ are respectively almost two times greater and at least three times greater than their values for the monolayer. This is the main result of this paper. The errors for the bilayer are the standard deviations of mean for the 14 values of $\Delta_{\rm imm}$ and $\Psi_{\rm imm}$ in Fig. 2. We verified that we obtain the same results using the experimental data $\Delta_{\rm sub}$ and $\Psi_{\rm sub}$ either at $\theta = 45^\circ$, and either at 60°.

The theoretical fits in Fig. 2 are those obtained once we set $\chi_\parallel$, $\chi_\perp$, $\sigma_\parallel$, $\sigma_\perp$ equal to the bilayer values of Table I in the reflection coefficients. The same holds for the two curves (solid and dashed line) that fit the experimental data in Fig. 3. The patterned area at -45° in Fig. 3 is the theoretical predictions for $R_{\rm p\_imm}(\theta)$ if we let $\chi_\parallel$, $\chi_\perp$, $\sigma_\parallel$ equal to the bilayer values of Table I while we set $\sigma_\perp$ compatible with the observations for the monolayer. The patterned area at 45° in the same figure shows the theoretical predictions if we further choose $\chi_\perp$ equal to the value observed for the monolayer. This shows how the variation of the out-of-plane optical constants of bilayer graphene with respect to the monolayer affects $R_{\rm p\_imm}(\theta)$. A larger value of $\chi_\perp$ shifts $\theta_{\rm pB}$ at lower values, and a larger value of $\sigma_\perp$ rises the value of $R_{\rm p\_imm}(\theta_{\rm pB})$.

Figure 5 shows the *ab initio* computations, based on the *GW*-BSE (Bethe-Salpeter equation) method which includes many-body effects, for $\chi_\perp$ and $\sigma_\perp$ in bilayer graphene. These physical quantities have been evaluated using an approach [33,34] similar to those used in Refs. [11,12,16]. We observe that the values computed at $\lambda = 633$ nm compare

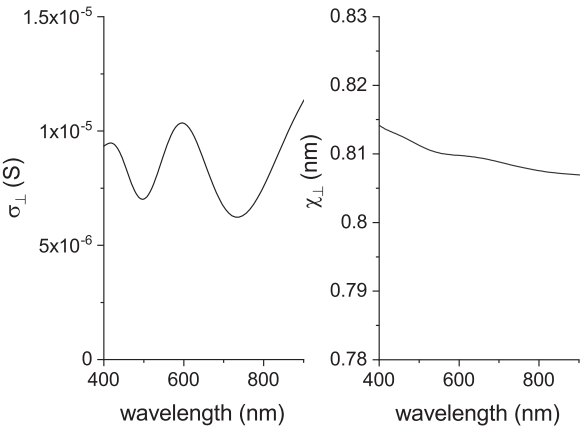

FIG. 5. *Ab initio* calculations of $\chi_\perp$ and $\sigma_\perp$ for bilayer graphene in the optical spectrum.

well with the experimental data that we report. This is another confirmation of the good quality of our experimental results. In particular, if we compare these theoretical values with those obtained for the monolayer [11,12,16], *ab initio* calculations confirm that the out-of-plane optical constants of bilayer graphene are way different than what is observed for the monolayer.

We analyzed the experimental data based on formulas that, in our opinion, provide the exact Fresnel reflection coefficients of a bilayer. Intuitively, we can expect that the multiple reflections in between the two atomic layers (Fig. 4) play a small role here. We verified it by repeating the data analysis using the formulas for the monolayer [formulas (3) and (4) of Ref. [16] for *p*-polarized light, and formula (6) of Ref. [35] for *s*-polarized light]. In this case, of course, having a single layer, we obtain $\chi_\parallel$, $\chi_\perp$, $\sigma_\parallel$, $\sigma_\perp$ that are double those of Table I. Within our experimental precision this second approach is equivalent to the exact one.

V. DISCUSSION AND CONCLUSION

In his Nobel lecture, Novoselov says that, "Although the addition of one layer on top of graphene is all that is needed to arrive at bilayer graphene, the properties of the latter are not simply twice those of the monolayer crystal; this is one of those cases where one plus one is greater than two" [36]. Bilayer graphene fully confirms this statement for electrostatics [37] and even for the very basic properties of linear optics. While for *s*-polarized light the Fresnel reflection coefficient of bilayer graphene immersed in a transparent dielectric or in vacuum is practically twice the one for the monolayer, for *p* polarization it is completely different (Fig. 3). This because the out-of-plane optical constants of bilayer graphene are remarkably different compared to the monolayer. We proved this experimentally and our results are confirmed by *ab initio* calculations.

We have measured $\sigma_\perp$ at optical frequencies in bilayer graphene. Together with $\chi_\perp$ these are basic properties that strongly influence the light-matter interaction in 2D crystals starting from the reflectivity response. The out-of-plane optical constants have proven difficult to observe. We predict that our paper will stimulate experimental efforts in a complete

characterization of the optical constants of 2D materials that until now has been limited mostly to the in-plane optical constants [2,3,6,18,20]. Results reported in this paper are relative to bilayer graphene at $\lambda = 633$ nm but the measurements are easily extended to other materials and to other wavelengths.

We expect that the out-of-plane optical constants of 2D materials will be of the utmost importance in a careful description of the linear [38] and the nonlinear [39] optical phenomena associated to these crystals. Among possible applications, 2D materials have been proposed as optical modulators [40,41]. The out-of-plane properties are expected to play a role when non-normal incidence is required [42]. Photonic integrated circuits can benefit from the giant out-of-plane optical anisotropy in TMDC thin films [7]. In monolayer TMDC, this anisotropy will be even greater than in the bulk materials. Monolayer or few-layer waveguides for on-chip photonics have been recently developed, showing millimeter-scale light transport in a 2D waveguide [38,43]. In the same context, it was shown how optical anisotropy, perpendicular to the atomic layers, offers new opportunities and novel control knobs when designing 2D photonic integrated circuits [43,44]. For these reasons the archive of light-matter interactions in atomically thin materials should include as soon as possible a complete experimental and theoretical characterization of their out-of-plane optical properties.

ACKNOWLEDGMENTS

M.M. acknowledges financial support from PARD_UNIPD Contract No. MERA_BIRD 23_01, and L.D. acknowledges financial support from PNRR Decreto Ministeriale 118 del 02-03-2023. D.F. and L.C. prepared the PDMS substrate and prism, Y.H., Z.X., A.M., and M.M. did the optical measurements and data analysis, L.D.A. and M.M. composed the analytical theory, P.U. ran the *ab initio* calculations, M.M. conceived the idea for the paper and drafted this manuscript, and then the manuscript was read, improved, and finally acknowledged by the other authors.

APPENDIX: REFLECTION COEFFICIENTS

Willing to compute $r_{p\parallel}$, the boundary conditions are [10,16]

$$\begin{aligned}&\hat{\kappa}\times(\vec{E}_{\mathrm{II}1(2)}-\vec{E}_{\mathrm{I}1(2)})=0,\\&\hat{\kappa}\times(\vec{H}_{\mathrm{II}1(2)}-\vec{H}_{\mathrm{I}1(2)})=i\omega P_{1(2)y}\hat{j}+J_{1(2)y}\hat{j},\end{aligned}\tag{A1}$$

where the subscript I (II) stands for the field immediately above (below) each atomic layer. We need then to solve this linear system of eight equations,

$$E_{yi}-E_{yr}=E_{y+}-E_{y-},\tag{A2}$$

$$E_{y+}e^{-i\beta}-E_{y-}e^{i\beta}=E_{yt},\tag{A3}$$

$$H_{xi}+H_{xr}=H_{x+}+H_{x-}+i\omega P_{1y}+J_{1y},\tag{A4}$$

$$H_{x+}e^{-i\beta}+H_{x-}e^{i\beta}=H_{xt}+i\omega P_{2y}+J_{2y},\tag{A5}$$

$$E_{yi}-E_{yr}=\frac{P_{1y}}{\epsilon_0\chi_\parallel},\quad E_{yt}=\frac{P_{2y}}{\epsilon_0\chi_\parallel},\tag{A6}$$

$$E_{yi}-E_{yr}=\frac{J_{1y}}{\sigma_\parallel},\quad E_{yt}=\frac{J_{2y}}{\sigma_\parallel},\tag{A7}$$

where $\beta=n\frac{2\pi d}{\lambda}\cos\theta$. Equations (A2)–(A5) come from the boundary conditions [Eq. (A1)] for the electric and the magnetic fields at the two atomic planes, and Eqs. (A6) and (A7) come from the definitions (3) and (4). We have $r_{p\parallel}=H_{xr}/H_{xi}$.

For $r_{p\perp}$ the boundary conditions are [10,16]

$$\begin{aligned}&\hat{\kappa}\times(\vec{E}_{II1(2)}-\vec{E}_{I1(2)})=-\frac{\hat{\kappa}}{\epsilon_0}\times\mathrm{grad}\left(P_{1(2)z}+\frac{J_{1(2)z}}{i\omega}\right),\\&\hat{\kappa}\times(\vec{H}_{II1(2)}-\vec{H}_{I1(2)})=0.\end{aligned}\tag{A8}$$

We have

$$E_{yi}-E_{yr}=E_{y+}-E_{y-}+\frac{ik\sin\theta}{\epsilon_0}\left(P_{1z}+\frac{J_{1z}}{i\omega}\right),\tag{A9}$$

$$E_{y+}e^{-i\beta}-E_{y-}e^{i\beta}=E_{yt}+\frac{ik\sin\theta}{\epsilon_0}\left(P_{2z}+\frac{J_{2z}}{i\omega}\right),\tag{A10}$$

$$H_{xi}+H_{xr}=H_{x+}+H_{x-},\tag{A11}$$

$$H_{x+}e^{-i\beta}+H_{x-}e^{i\beta}=H_{xt},\tag{A12}$$

$$E_{zi}+E_{zr}=\frac{P_{1z}}{\epsilon_0\chi_\perp},\quad E_{zt}=\frac{P_{2z}}{\epsilon_0\chi_\perp},\tag{A13}$$

$$E_{zi}+E_{zr}=\frac{J_{1z}}{\sigma_\perp},\quad E_{zt}=\frac{J_{2z}}{\sigma_\perp},\tag{A14}$$

where these equations have the same meaning as in the previous case and the solution H_{xr} for this system fixes $r_{p\perp}=H_{xr}/H_{xi}$.

For s polarization the boundary conditions are

$$\begin{aligned}&\hat{\kappa}\times(\vec{E}_{II1(2)}-\vec{E}_{I1(2)})=0,\\&\hat{\kappa}\times(\vec{H}_{II1(2)}-\vec{H}_{I1(2)})=i\omega P_{1(2)y}\hat{i}+J_{1(2)y}\hat{i}.\end{aligned}\tag{A15}$$

The system of eight equations now runs,

$$E_{xi}+E_{xr}=E_{x+}+E_{x-},\tag{A16}$$

$$E_{x+}e^{-i\beta}+E_{x-}e^{i\beta}=E_{xt},\tag{A17}$$

$$H_{yi}-H_{yr}=H_{y+}-H_{y-}+i\omega P_{1x}+J_{1x},\tag{A18}$$

$$H_{y+}e^{-i\beta}-H_{y-}e^{i\beta}=H_{yt}+i\omega P_{2x}+J_{2x},\tag{A19}$$

$$E_{xi}+E_{xr}=\frac{P_{1x}}{\chi_\parallel\epsilon_0},\quad E_{xt}=\frac{P_{2x}}{\chi_\parallel\epsilon_0},\tag{A20}$$

$$E_{xi}+E_{xr}=\frac{J_{1x}}{\sigma_\parallel},\quad E_{xt}=\frac{J_{2x}}{\sigma_\parallel},\tag{A21}$$

and the Fresnel reflection coefficient is $r_{\mathrm{s\_imm}}=\frac{E_{rx}}{E_{ix}}$.

We measured also the bilayer graphene deposited on a PDMS substrate, so $r_{\mathrm{p\_sub}}$ and $r_{\mathrm{s\_sub}}$ can be computed with the same systems of linear equations, with these minor variations: $\beta=\frac{2\pi d}{\lambda}\cos\theta$, $\eta\vec{H}_a=\hat{s_a}\times\vec{E}_a$ for all the electromagnetic fields except for the transmitted one for which we have $\frac{\eta}{n}\vec{H}_t=\hat{s_t}\times\vec{E}_t$ where, for Snell's law, $\hat{s_t}=(0,-\sin\theta_t,\cos\theta_t)$ with $n\sin\theta_t=\sin\theta$. Finally, in accordance with the superposition principle for p polarization, $r_{\mathrm{p\_sub}}=r_{p\parallel}+r_{p\perp}-r_{\mathrm{p\_substrate}}$ because the reflection coefficient of the bare substrate $r_{\mathrm{p\_substrate}}$ is counted twice in our equations.

[1] P. Blake, E. W. Hill, A. H. Castro Neto, K. S. Novoselov, D. Jiang, R. Yang, T. J. Booth, and A. K. Geim, Making graphene visible, Appl. Phys. Lett. **91**, 063124 (2007).

[2] Y. Li, A. Chernikov, X. Zhang, A. Rigosi, H. M. Hill, A. M. van der Zande, D. A. Chenet, E.-M. Shih, J. Hone, and T. F. Heinz, Measurement of the optical dielectric function of monolayer transition-metal dichalcogenides: MoS_2, $MoSe_2$, WS_2, and WSe_2, Phys. Rev. B **90**, 205422 (2014).

[3] G. A. Ermolaev, Y. V. Stebunov, A. A. Vyshnevyy, D. E. Tatarkin, D. I. Yakubovsky, S. M. Novikov, D. G. Baranov, T. Shegai, A. Y. Nikitin, A. V. Arsenin, and V. S. Volkov, Broadband optical properties of monolayer and bulk MoS_2, NPJ 2D Mater. Appl. **4**, 21 (2020).

[4] B. T. Draine, Graphite revisited, Astrophys. J. **831**, 109 (2016).

[5] G. E. Jellison, J. D. Hunn, and H. N. Lee, Measurement of optical functions of highly oriented pyrolytic graphite in the visible, Phys. Rev. B **76**, 085125 (2007).

[6] K. M. Islam, R. Synowicki, T. Ismael, I. Oguntoye, N. Grinalds, and M. D. Escarra, In-plane and out-of-plane optical properties of monolayer, few-layer, and thin-film MoS_2 from 190 to 1700 nm and their application in photonic device design, Adv. Photonics **2**, 2000180 (2021).

[7] G. A. Ermolaev, D. V. Grudinin, Y V. Stebunov, K. V. Voronin, V. G. Kravets, J. Duan, A. B. Mazitov, G. I. Tselikov, A. Y. Bylinkin, D. G. Yakubovsky, S. M. Novikov, D. G. Baranov, A. Y. Nikitin, I. A. Kruglov, T. Shegai, P. Alonso-Gonzalez, A. N. Grigorenko, A. V. Arsenin, K. S. Novoselov, and V. S. Volkov, Giant optical anisotropy in transition metal dichalcogenides for next-generation photonics, Nat. Commun. **12**, 854 (2021).

[8] R. Geick, C. H. Perry, and G. Rupprecht, Normal modes in hexagonal boron nitride, Phys. Rev. **146**, 543 (1966).

[9] F. J. Nelson, V. K. Kamineni, T. Zhang, E. S. Comfort, J. U. Lee, and A. C. Diebold, Optical properties of large-area polycrystalline chemical vapor deposited graphene by spectroscopic ellipsometry, Appl. Phys. Lett. **97**, 253110 (2010).

[10] L. Dell'Anna, Y. He, and M. Merano, Reflection, transmission, and surface susceptibility tensor of two-dimensional materials, Phys. Rev. A **105**, 053515 (2022).

[11] P. E. Trevisanutto, M. Holzmann, M. Côté, and V. Olevano, *Ab initio* high-energy excitonic effects in graphite and graphene, Phys. Rev. B **81**, 121405(R) (2010).

[12] I. Guilhon, M. Marques, L. K. Teles, M. Palummo, O. Pulci, S. Botti, and F. Bechstedt, Out-of-plane excitons in two-dimensional crystals, Phys. Rev. B **99**, 161201(R) (2019).

[13] B. Majérus, E. Dremetsika, M. Lobet, L. Henrard, and P. Kockaert, Electrodynamics of two-dimensional materials: Role of anisotropy, Phys. Rev. B **98**, 125419 (2018).

[14] B. Majérus, L. Henrard, and P. Kockaert, Optical modeling of single and multilayer two-dimensional materials and heterostructures, Phys. Rev. B **107**, 045429 (2023).

[15] A. Laturia, M. L. Van de Put, and W. G. Vandenberghe, Dielectric properties of hexagonal boron nitride and transition metal dichalcogenides: from monolayer to bulk, NPJ 2D Mater. Appl. **2**, 6 (2018).

[16] Z. Xu, D. Ferraro, A. Zaltron, N. Galvanetto, A. Martucci, L. Sun, P. Yang, Y. Zhang, Y. Wang, Z. Liu, J. D. Elliott, M. Marsili, L. Dell'Anna, P. Umari, and M. Merano, Optical detection of the susceptibility tensor in two-dimensional crystals, Commun. Phys. **4**, 215 (2021).

[17] Z. Xu, D. Ferraro, Y. He, A. Zaltron, N. Galvanetto, L. Sun, Y. Wang, J. Wu, J. Dong, P. Yang, Y. Zhang, Z. Liu, and M. Merano, Pseudo-Brewster angles for monolayer-MoS_2 and graphene immersed in a dielectric medium, Thin Solid Films **761**, 139491 (2022).

[18] B. Song, H. Gu, S. Zhu, H. Jiang, X. Chen, C. Zhang, and S. Liu, Broadband optical properties of graphene and HOPG investigated by spectroscopic Mueller matrix ellipsometry, Appl. Surf. Sci. **439**, 1079 (2018).

[19] R. Kenaz, S. Ghosh, P. Ramachandran, K. Watanabe, T. Taniguchi, H. Steinberg, and R. Rapaport, Thickness mapping and layer number identification of exfoliated van der Waals materials by Fourier imaging micro-ellipsometry, ACS Nano **17**, 9188 (2023).

[20] J. D. Elliott, Z. Xu, P. Umari, G. Jayaswal, M. Chen, X. Zhang, A. Martucci, M. Marsili, and M. Merano, Surface susceptibility and conductivity of MoS_2 and WSe_2 monolayers: A first-principles and ellipsometry characterization, Phys. Rev. B **101**, 045414 (2020).

[21] R. Frisenda, Y. Niu, P. Gant, A. J. Molina-Mendoza, R. Schmidt, R. Bratschitsch, J. Liu, L. Fu, D. Dumcenco, A. Kis, D. P. De lara, and A. Castellanos-Gomez, Micro-reflectance and transmittance spectroscopy: A versatile and powerful tool to characterize 2D materials, J. Phys. D: Appl. Phys. **50**, 074002 (2017).

[22] D. Bing, Y. Wang, J. Bai, R. Du, G. Wu, and L. Liu, Optical contrast for identifying the thickness of two-dimensional materials, Opt. Commun. **406**, 128 (2018).

[23] R. R. Nair, P. Blake, A. N. Grigorenko, K. S. Novoselov, T. J. Booth, T. Stauber, N. M. R. Peres, and A. K. Geim, Fine structure constant defines visual transparency of graphene, Science **320**, 1308 (2008).

[24] M. A. El-Sayed, G. A. Ermolaev, K. V. Voronin, R. I. Romanov, G. I. Tselikov, D. I. Yakubovsky, N. V. Doroshina, A. B. Nemtsov, V. R. Solovey, A. A. Voronov, S. M. Novikov, A. A. Vyshnevyy, A. M. Markeev, A. V. Arsenin, and V. S. Volkov, Optical constants of chemical vapor deposited graphene for photonic applications, Nanomaterials **11**, 1230 (2021).

[25] S.-E. Zhu, S. Yuan, and G. C. A. M. Janssen, Optical transmittance of multilayer graphene, Europhys. Lett. **108**, 17007 (2014).

[26] M. Bruna and S. Borini, Optical constants of graphene layers in the visible range, Appl. Phys. Lett. **94**, 031901 (2009).

[27] V. G. Kravets, A. N. Grigorenko, R. R. Nair, P. Blake, S. Anissimova, K. S. Novoselov, and A. K. Geim, Spectroscopic ellipsometry of graphene and an exciton-shifted van Hove peak in absorption, Phys. Rev. B **81**, 155413 (2010).

[28] D. den Engelsen, Ellipsometry of anisotropic films, J. Opt. Soc. Am. **61**, 1460 (1971).

[29] L. Dell'Anna and M. Merano, Clausius-Mossotti Lorentz-Lorenz relations and retardation effects for two-dimensional crystals, Phys. Rev. A **93**, 053808 (2016).

[30] L. Dell'Anna and M. Merano, Optical response of a bilayer crystal, Phys. Rev. A **99**, 013802 (2019).

[31] E. D. Palik, *Handbook of Optical Constants of Solids II*, 1st ed. (Academic Press, San Diego, 1991), pp. 449–460.

[32] N. Chen, S. Rabii, and N. Holzwarth, Calculation of the optical spectra for graphite, Synth. Met. **8**, 197 (1983).

[33] G. Prandini, M. Galante, N. Marzari, and P. Umari, SIMPLE code: Optical properties with optimal basis functions, Comput. Phys. Commun. **240**, 106 (2019).

[34] P. Umari, A fully linear response G_0W_0 method that scales linearly up to tens of thousands of cores, J. Phys. Chem. A **126**, 3384 (2022).

[35] M. Merano, Fresnel coefficients of a two-dimensional atomic crystal, Phys. Rev. A **93**, 013832 (2016).

[36] K. Novoselov, Nobel Lecture, https://www.nobelprize.org/prizes/physics/2010/novoselov/lecture/ (2010).

[37] S. Slizovskiy, A. Garcia-Ruiz, A. I. Berdyugin, N. Xin, T. Taniguchi, K. Watanabe, A. K. Geim, N. D. Drummond, and V. I. Fal'ko, Out-of-plane dielectric susceptibility of graphene in twistronic and Bernal bilayers, Nano Lett. **21**, 6678 (2021).

[38] M. Lee, H. Hong, J. Yu, F. Mujid, A. Ye, C. Liang, and J. Park, Wafer-scale δ waveguides for integrated two-dimensional photonics, Science **381**, 648 (2023).

[39] E. Dremetsika and P. Kockaert, Enhanced optical Kerr effect method for a detailed characterization of the third-order nonlinearity of two-dimensional materials applied to graphene, Phys. Rev. B **96**, 235422 (2017).

[40] Q.-Y. Wen, W. Tian, Q. Mao, Z. Chen, W.-W. Liu, Q.-H. Yang, M. Sanderson, and H.-W. Zhang, Graphene based all-optical spatial terahertz modulator, Sci. Rep. **4**, 7409 (2014).

[41] H. Chen, C. Wang, H. Ouyang, Y. Song, and T. Jiang, All-optical modulation with 2D layered materials: status and prospects, Nanophotonics **9**, 2107 (2020).

[42] V. G. Kravets, F. Wu, G. H. Auton, T. Yu, S. Imaizumi, and A. N. Grigorenko, Measurements of electrically tunable refractive index of MoS_2 monolayer and its usage in optical modulators, NPJ 2D Mater. Appl. **3**, 36 (2019).

[43] L. Wu, Ultrathin waveguides for 2D photonic integrated circuits, Nat. Rev. Phys. **5**, 634 (2023).

[44] A. A. Vyshnevyy, G. A. Ermolaev, D. V. Grudinin, K. V. Voronin, I. Kharichkin, A. Mazitov, I. A. Kruglov, D. I. Yakubovsky, P. Mishra, R. V. Kirtaev, A. V. Arsenin, K. S. Novoselov, L. Martin-Moreno, and V. S. Volkov, van der Waals materials for overcoming fundamental limitations in photonic integrated circuitry, Nano Lett. **23**, 8057 (2023).